ACS APPLIED ENERGY MATERIALS

www.acsaem.org Article

Molecularly Engineered Low-Cost Organic Hole-Transporting Materials for Perovskite Solar Cells: The Substituent Effect on Non-fused Three-Dimensional Systems

Desire Molina, Esmaeil Sheibani,* Bowen Yang, Hajar Mohammadi, Maryam Ghiasabadi, Bo Xu, Jiajia Suo, Brian Carlsen, Nick Vlachopoulos, Shaik Mohammed Zakeeruddin, Michael Grätzel, and Anders Hagfeldt*

Cite This: *ACS Appl. Energy Mater.* 2022, 5, 3156–3165 Read Online

ACCESS | Metrics & More | Article Recommendations | Supporting Information

ABSTRACT: In this work, we describe a new class of non-fused 3D asymmetric compounds (named **1**, **2**, **3**, and **4**) as low-cost organic hole-transporting materials (HTMs) for perovskite solar cells (PSCs). The fundamental understanding of the influence of the methylthio and methoxy group substitutions on the fluorene moiety has been analyzed, as well as the position of methoxy groups in the aromatic rings of triphenylamine pending groups (*para* or *meta*). Experimental results demonstrate that the position of the methoxy group in the triphenylamine pending group influences decisively the thermal properties and the amplitude of the electronic bandgap, hydrophobicity, film formation, and thermal stress stability. The presence of methylthio or methoxyl substituents in the 2,7-positions of the fluorene moiety mainly affects the electrochemical properties, hole mobility, and morphology of the hole-transporting layer (HTL). Thus, maxima sunlight-to-electricity power conversion efficiencies (PCEs) of 17.7 and 17.8% have been obtained in PSCs with methoxy groups in the fluorene moieties (**1** and **3**), respectively. Consequently, compound **1**-based PSCs exhibit a better stability than the other three materials and the standard HTM-spiro-OMeTAD-based devices.

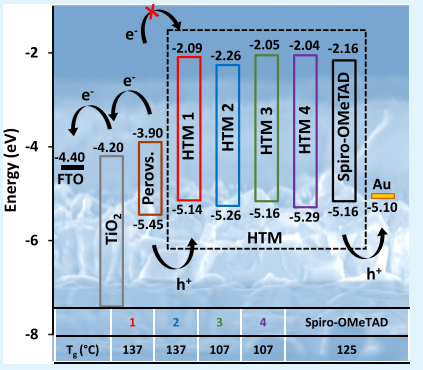

KEYWORDS: *hole-transporting materials, perovskite solar cells, 3D non-fused fluorene structure, low-cost, stability*

HIGHLIGHT

- Four cost-effective, feasibly synthesized, and asymmetric hole-transporting materials are designed and applied for PSCs.
- The influence of the sulfur and oxygen group substitutions on the twisted structural of HTMs on photophysical and electrochemical properties has been thoroughly scrutinized.
- An efficient hole-transporting material **1** shows a remarkable photovoltaic performance, stability, and hydrophobicity, which demonstrate the proficiency of **1** as a favorable candidate to replace prototype spiro-OMeTAD.

INTRODUCTION

Perovskite solar cells (PSCs) have stirred up a large volume of research over the past few years due to their outstanding photovoltaic performance and potential for commercialization.[1,2] Nevertheless, some of the obstacles that must still be overcome in order to reach the marketing of these devices are long-term stability and the cost of materials. For this purpose, most studies are invested in optimizing the compositional engineering of the perovskite layer,[3−6] developing different device architectures[7−10] and various deposition techniques, and designing new practical hole-transporting materials (HTMs) and electron-transporting materials (ETMs).[11−13] Thus far, a wide range of HTMs based on small organic molecules has been explored on PSCs with different core structures such as carbazole,[14−16] perylene,[17,18] thiophene,[19] spiro,[15,20−22] helicene,[23] phenoxazine,[24,25] and triphenylamine.[26−28] Among them, 2,2′,7,7′-tetrakis(*N*,*N*-di-*p*-methoxyphenylamine)-9,9′-spirobifluorene (spiro-OMeTAD) is continuously used as a popular reference HTM to tune the device operational condition. Although it is a material that provides good efficiency, it suffers from severe problems including complicated and expensive synthesis, lack of stability, and hydrophilicity, as well as being prone to a phase transition from the amorphous to the crystalline state.[29] All of these have

Received: December 1, 2021
Accepted: February 9, 2022
Published: February 18, 2022

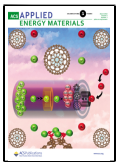

https://doi.org/10.1021/acsaem.1c03775
ACS Appl. Energy Mater. 2022, 5, 3156−3165

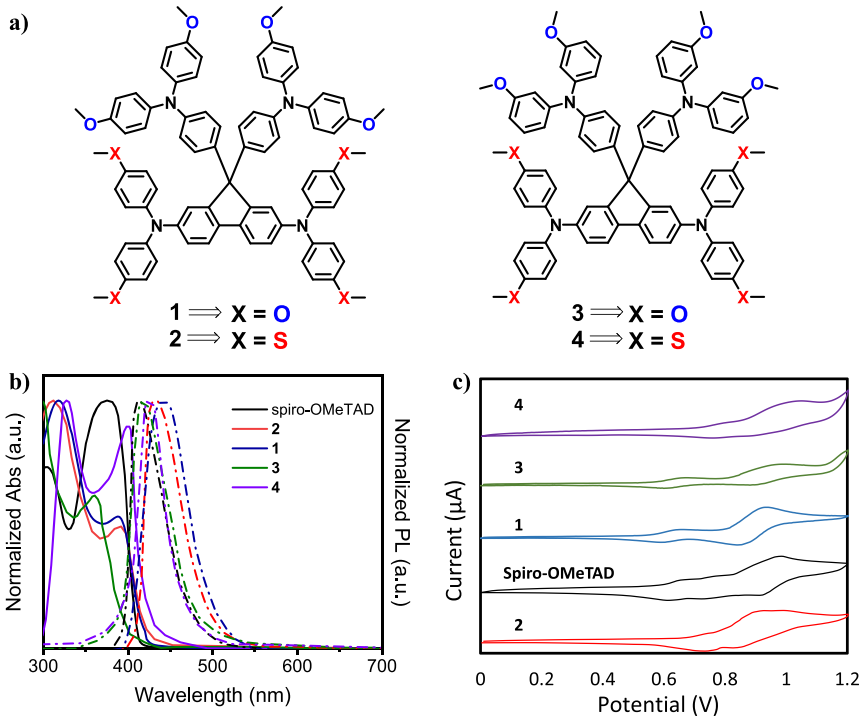

Figure 1. (a) Molecular structures of HTMs **1**, **2**, **3**, and **4**. (b) Normalized UV−Visible absorption and photoluminescence of **1**, **2**, **3**, **4**, and spiro-OMeTAD in DCM (10^{-5} M). (c) Cyclic voltammograms of HTMs **1**, **2**, **3**, **4**, and spiro-OMeTAD (in DCM, 10^{-4} M).

Table 1. Electrochemical, Optical, and Thermal Parameters and Hole Mobilities of Different HTMs

HTM	λ_{abs} (nm)	$E_{opt.gap}$ (eV)[b]	E_{ox1} (eV)	HOMO (eV)[a]	LUMO (eV)	T_g (°C)[c]	μ_h (cm^2V^{-1} s^{-1})[d]
spiro-OMeTAD	303,386	3.00	0.64	−5.16	−2.16	125	9.10×10^{-5}
1	318,392	3.05	0.63	−5.14	−2.09	137	1.46×10^{-5}
2	312,392	3.00	0.74	−5.26	−2.26	137	2.76×10^{-6}
3	300,365	3.11	0.64	−5.16	−2.05	107	1.50×10^{-5}
4	320,395	3.25	0.78	−5.29	−2.04	107	1.13×10^{-6}

[a]LUMO−HOMO band gap of the hole conductor determined from the intersection of the normalized emission and absorption spectra. [b]Determined by solution-based cyclic voltammetry (CV), 0.1 M *n*-tetrabutylammoniun hexafluorophosphate ($TBAPF_6$) as an electrolyte in dichloromethane solution; the reference electrode, in all cases, is aqueous Ag/AgCl (3 M KCl), separated from the working electrode compartment by a salt bridge containing the same electrolyte as the working electrode compartment. The working electrode was a glassy carbon disk (diameter: 3 mm); a platinum wire was used as the counter electrode, dipped in the same electrolyte as the working electrode. The cyclovoltammetric scan rate was 50 mV/s. All redox potentials were calibrated *vs* vacuum by the addition of ferrocene, with a conversion factor of $E_{(Fc/Fc^+)}$ = 624 mV *vs* SHE.[45] [c]Glass transition temperature measured by differential scanning calorimetry (DSC). [d]Hole mobility determined by the space-charge limiting current technique.

incited scientists to devote substantial efforts toward the development of alternative HTMs without the aforementioned problems and with the additional advantage of producibility at low costs in the industrial scale. Toward this goal, an enormous number of HTMs based on different structural aspects such as a planar,[30−32] star-shaped,[33] linear D-A, or discotic D-A-D[34] have been reported. Although several attempts have been made to introduce new HTMs for PSCs, most often with a remarkable efficiency, there is no clear relationship between the chemical structure of the HTM molecule and the charge transport efficiency. Therefore, it is still critical to design new molecular structures adapted to the needs of the perovskite solar cell field. Very recently, we introduced species with the carbazole 3D structure as a new alternative to obtain an in-depth understanding of the impact of intramolecular π-conjugation on device efficiency.[35] Notably, we thoroughly described the influence of carbazole on the photovoltaic parameters even though the respective sunlight-to-electricity power conversion efficiency (PCE) is slightly lower than in the case of spiro-OMeTAD. Inspired by this approach, we designed and synthesized four new 3D aminofluorene-based structures containing 4- and/or 3-methoxyphenyle and/or 4-methylthiophenyle groups in the amine nitrogen based on enhanced structural tenacity (**1**, **2**, **3**, and **4**). These derivatives have been synthesized from cheap and abundant reagents, such as aniline, dibromofluorene, and iodoanisole. In addition, to avoid the disadvantages of spiro-OMeTAD in terms of its high symmetry, the new materials that are introduced here have a spirofluorene structure, in which a carbon−carbon bond has been broken to give the structure greater conformational freedom and, therefore, less degree of symmetry. The main objective of this work is to know how the presence of methoxy and/or methylthio groups and their position in the ring affect the optoelectronic properties of these derivatives, as well as the properties as HTMs of these new materials.

https://doi.org/10.1021/acsaem.1c03775
ACS Appl. Energy Mater. 2022, 5, 3156−3165

RESULTS AND DISCUSSION

Synthesis. The synthesis of the four new derivatives involved three steps (Scheme S1 and Figure 1a). The first reaction was the Buchwald−Hartwig coupling of aniline with iodoanisole to get methoxytriphenylamine units, which are covalently linked to the dibromofluorene core by a condensation reaction with ketone under acidic conditions. Finally, the four derivatives were obtained after a last Buchwald−Hartwig reaction with high yields (76, 85, 82, and 78% for **3**, **4**, **2**, and **1**, respectively). It should be noted that only in the second step, the intermediate was purified by column chromatography. In the other two steps, purification was carried out by crystallization, which reduced the cost of the target HTMs. Additionally, not any limiting condition was applied, such as the toxic reagent, Grignard reaction, and other reactions involving corrosive reagents that are used for spiro-OMeTAD synthesis. Cost analysis for the preparation of new HTMs **1**, **2**, and **3** demonstrates a subnational improvement in price 16.36, 19.41, and 23.85 $/g, respectively, which are nearly 25 times lower than that of the synthesis of spiro-OMeTAD (around 471.09 $/g).[36] The detailed material quantities are summarized in Tables S3−S10. All these compounds showed good solubility in all of the common organic solvents, which are fundamentally critical for the solution-based process technique HTM deposition on PSCs. Complete structural characterization including ^{1}H NMR, ^{13}C NMR, UV−Vis, HRMS, DSC, and TGA of the compounds was fulfilled (see the Supporting Information).

Thermal Properties. The thermal behaviors of new HTMs were measured by differential scanning calorimetry (DSC) and thermogravimetric analysis (TGA) with detailed information that is summarized in Table 1. All new materials demonstrated a decomposition temperature (T_d) over 370 °C (Figures S15−S18), indicating that they are suitable materials for application in photovoltaic technologies. A notable change in the glass transition feature happens as a result of the oxygen location in the aromatic rings of triphenylamine pending groups, which is directly connected to the fluorene core structure. Both **3** and **4** show similar T_g at 107 °C, while **1** and **2** display at 137 °C that is near to spiro-OMeTAD (125 °C).[37] The lower T_g of **3** and **4** might be attributed to more disordered molecular packing because of the *meta* substitution and less intermolecular interaction that consecutively leads to a lower compact film formation.[16] Thus, no difference was found in terms of thermal properties between the alkylthio-substituted fluorene and dialkoxy-fluorene moiety. This analysis reveals that the molecular structure has a crucial influence on the morphological stability of the amorphous films and simultaneously on the control of the tendency to crystallize upon heating.

DFT Calculations. In order to obtain more facts about the molecular geometry and electronic properties of new HTMs, quantum chemical calculations have been accomplished based on the B3LYP/6-31G** level (see the SI for computational details). The highest occupied molecular orbital (HOMO) and the lowest unoccupied molecular orbital (LUMO) levels of calculation are summarized in Table S1 and consistent with experimental measurement. As indicated in Table S1, both compounds **1** and **3** have the lowest reorganization energy that coincides with the higher hole mobility of these HTMs compared with HTMs **2** and **4** (Table 1). As the experimental results show, the spiro-OMeTAD molecule shows better hole-transporting properties than the new HTMs. DFT reveals that the spiro-OMeTAD has better and well-balanced charge-transfer properties as demonstrated by its λ and t values. In fact, the spiro-OMeTAD molecule exhibits relatively larger transfer integrals and smaller reorganization energies, resulting in larger charge transfer rates. For the sake of comparison, the experimental values for the hole mobilities are also included in Table S2. We also consider the face-to-face π-stacking geometry to approximately evaluate the carrier mobilities. Interestingly, the dimer spiro-OMeTAD molecule, with low reorganization energy and high transfer integral, represents the highest hole mobility. To obtain further insights into the electronic structures of the considered dimers, the HOMO and LUMO energy levels are depicted in Figure S2. For the two HTM **1** and **3** dimers, the distributions of HOMOs and LUMOs are almost similar to those observed for the single molecules. However, for the dimer spiro-OMeTAD, the HOMO and LUMO shapes indicate a diffused charge distribution. The delocalization of the HOMO and LUMO throughout the whole conjugated system suppresses carrier recombination, which facilitates the charge movement. Thus, the enhancement of transfer integrals in the spiro-OMeTAD molecule is mainly due to the increased effective orbital overlaps in this system, as shown in Figure S2.

Photophysical and Electrochemical Measurements. The absorption and emission spectra of the new HTMs and spiro-OMeTAD are depicted in Figure 1b and listed in Table 1. There is no vital difference observed in the absorption of the materials in dichloromethane solution. Two maximum absorptions (λ_{max}) are located at 306−320 and 390−395 nm with a shoulder band toward a higher wavelength, around 420 nm. The bathochromic shift of **1** might be ascribed to the presence of *para* electron-donating methoxy groups with the same p-orbital nature with the carbon atoms of the phenyl moiety that in turn caused sturdy delocalized intramolecular π-conjugation. The maximum fluorescence emission peaks (λ_{em}) of **1**, **2**, **3**, **4**, and spiro-OMeTAD are centered at 443, 414, 423, 414, and 446 nm respectively, which means that **1** shows the largest Stokes shifts with 53 nm. A more significant Stoke shift indicates that the HTM can tolerate more geometrical changes during excitation.[38] The UV−Vis spectra of the new solid-state materials were also measured (Figure S19). Derivatives **1** and **3** show the absorption maxima hypsochromically shifted with respect to derivatives **2** and **4** (310 and 394 nm for the first two, and 319 and 398 nm for the last, respectively). Each HTM, in its pristine form, exhibits absorption peaks in the UV and short wavelength visible range (<420 nm), which means that few incident photons can be absorbed by HTMs in this range, so they will not produce parasitic absorption to the detriment of the performance of the photovoltaic device. After chemical oxidation with a p-type oxidant during device operation, the oxidized HTM species show more extensively at the visible region.[39] The optical band gap is estimated from the intersection of normalized emission and absorption spectra, with related data collected in Table 1.

In order to estimate the energy levels of the new HTMs, cyclic voltammetry (CV) measurement has been performed in a dichloromethane (DCM) solution containing *n*-tetrabutylammonium hexafluorophosphate ($TBAPF_6$) as a supporting electrolyte and ferrocene as an internal standard under the same conditions, with the three-electrode system. HTMs containing methylthio groups display a much deeper oxidation potential compared to HTMs involving only methoxy groups. The corresponding data are collected in Table 1. A remarkable

https://doi.org/10.1021/acsaem.1c03775
ACS Appl. Energy Mater. 2022, 5, 3156−3165

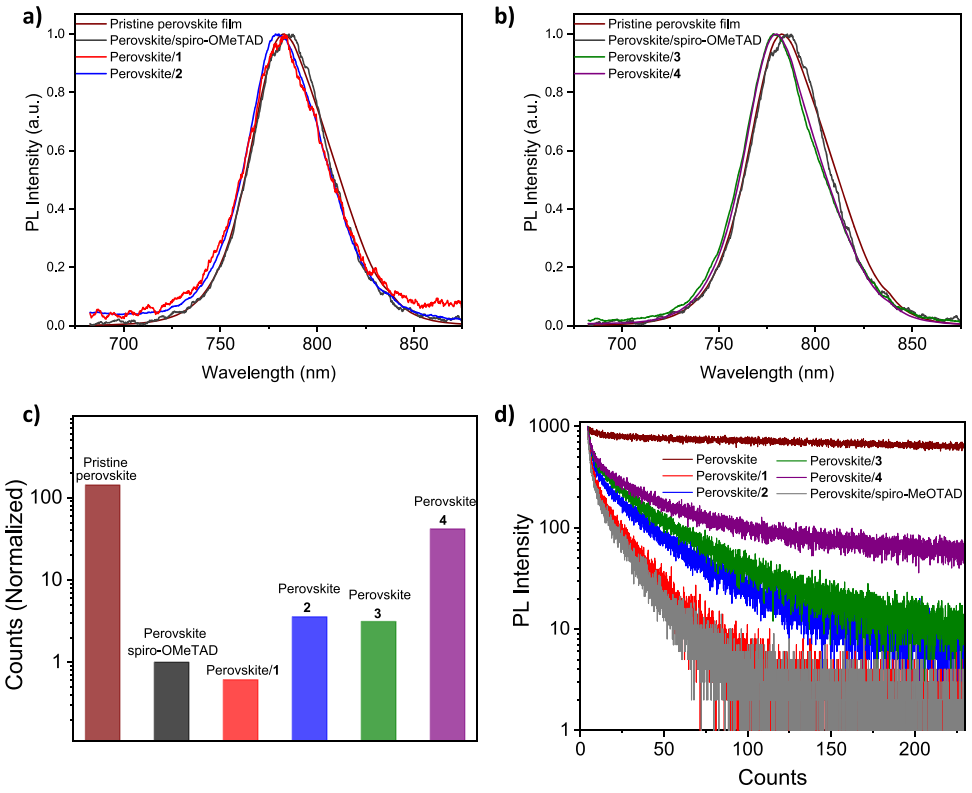

Figure 2. (a) Normalized steady-state PL curves of the pristine perovskite film, the perovskite/spiro-OMeTAD film with Li-TFSI and *t*BP, the perovskite/**1** film with Li-TFSI and *t*BP, and the perovskite/**2** film with Li-TFSI and *t*BP on a glass substrate. (b) Normalized steady-state PL curves of the pristine perovskite film, the perovskite/spiro-OMeTAD film with Li-TFSI and *t*BP, the perovskite/**3** film with Li-TFSI and *t*BP, and the perovskite/**4** film with Li-TFSI and *t*BP on a glass substrate. (c) Integrated PL spectra normalized to pristine perovskite. (d) TRPL spectra of the pristine perovskite film and perovskite/HTM films; excitation with 554 nm light was from the film side.

change (Figure 1c), by more than 100 meV in the electrochemical properties, occurs as a result of the substitution of sulfur at the bis(4-methylthiophenyl)amine in the fluorene and the methoxy *meta* substitution at the triphenylamine pending groups. Therefore, **4** shows the first oxidation potential (E_{ox1}) approximately at 0.78 eV, and the lowest E_{ox1} is related to **1** at 0.63 eV. Due to the HOMO energy levels of **2** and **4**, a higher open-circuit photovoltage (V_{oc}) than **1** is expected, even though V_{oc} is also influenced by surface recombination at the perovskite-HTM interface.[40−42] **2** and **4** show more negative HOMO levels than spiro-OMeTAD (−5.16 eV), while **1** and **3** present HOMOs close to that of the reference material (5.14 and −5.16 eV, respectively). The first overlapped oxidation peaks, which determine the HOMO, can be related to the oxidation reactions of bis(4-substituted phenyl)amine groups that directly connect to the fluorene core while the higher oxidation should be attributed to triphenylamine pending groups. According to the Hammett equation,[43] the second oxidation peaks of **3** and **4** are shifted to the positive direction owing to the position change from the *para* (resonance) to *meta* (inductive) position. The first oxidation potential of **1** shows a cathodic shift, especially compared to **2** and **4**, which indicates a strong electron donor character and leads to a higher HOMO energy level of −5.14 eV.[44] If we compare the structurally analogous materials **1**, **2**, **3**, and **4**, a larger band gap is observed for those with the methoxyl substituent groups in *meta* in the triphenylamine pending group.

To investigate the hole mobility of the different HTMs doped with lithium bis(trifluoromethanesulfonyl)imide (Li-TFSI) and *tert*-butylpyridine (*t*BP), the space-charge limited current (SCLC) was applied with a solution-processed thin film (Figure S20). The results are listed in Table 1. The hole mobility is lower in the films of the materials that present methylthio groups; this fact can be related to a thin layer morphology that favors less the charge mobility. In addition, all new materials have lower hole mobilities than the reference material. As reported previously, there is a trade-off between charge mobility and crystallization propensity. In fact, the new HTMs have a lower symmetry than spiro-OMeTAD, causing them to have a lesser tendency to crystallize that, in turn, could lead to low charge mobility.[46]

To gain a qualitative understanding of charge extraction, steady-state photoluminescence (ssPL) and time-resolved photoluminescence were performed. Luminescence occurs when an electron and hole recombine; thus, when comparing HTMs, a lower luminescence signal or faster decay time implies that more non-radiative recombination (NRR) is taking place. There are two mechanisms that may contribute to this: an increased number of interface defects, or a more effective hole extraction. While both mechanisms will quench the ssPL and time-resolved photoluminescence (TRPL) signals, an increase in defects will reduce the current under a given condition, while increased hole extraction will increase it.

In Figure 2a,b, the normalized steady-state ssPL spectra of the pristine perovskite film and the modified perovskite films with the doped HTMs under study are shown, with no significant change in spectral shape, indicating that the perovskite is not changed by the presence of the different HTMs, which is expected because HTMs barely absorb at

https://doi.org/10.1021/acsaem.1c03775
ACS Appl. Energy Mater. 2022, 5, 3156−3165

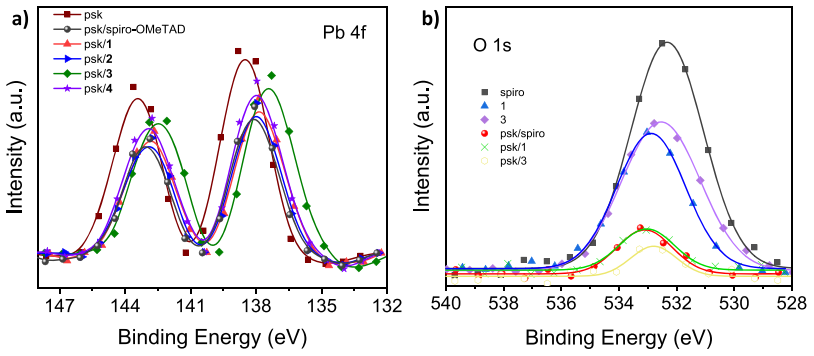

Figure 3. (a) Pb 4f signal from the spiro-OMeTAD-, **1**-, **2**-, **3**-, and **4**-coated perovskite samples compared to pristine samples. (b) O 1s signals from the spiro-OMeTAD-, **1**-, and **3**-coated perovskite samples compared to pristine samples.

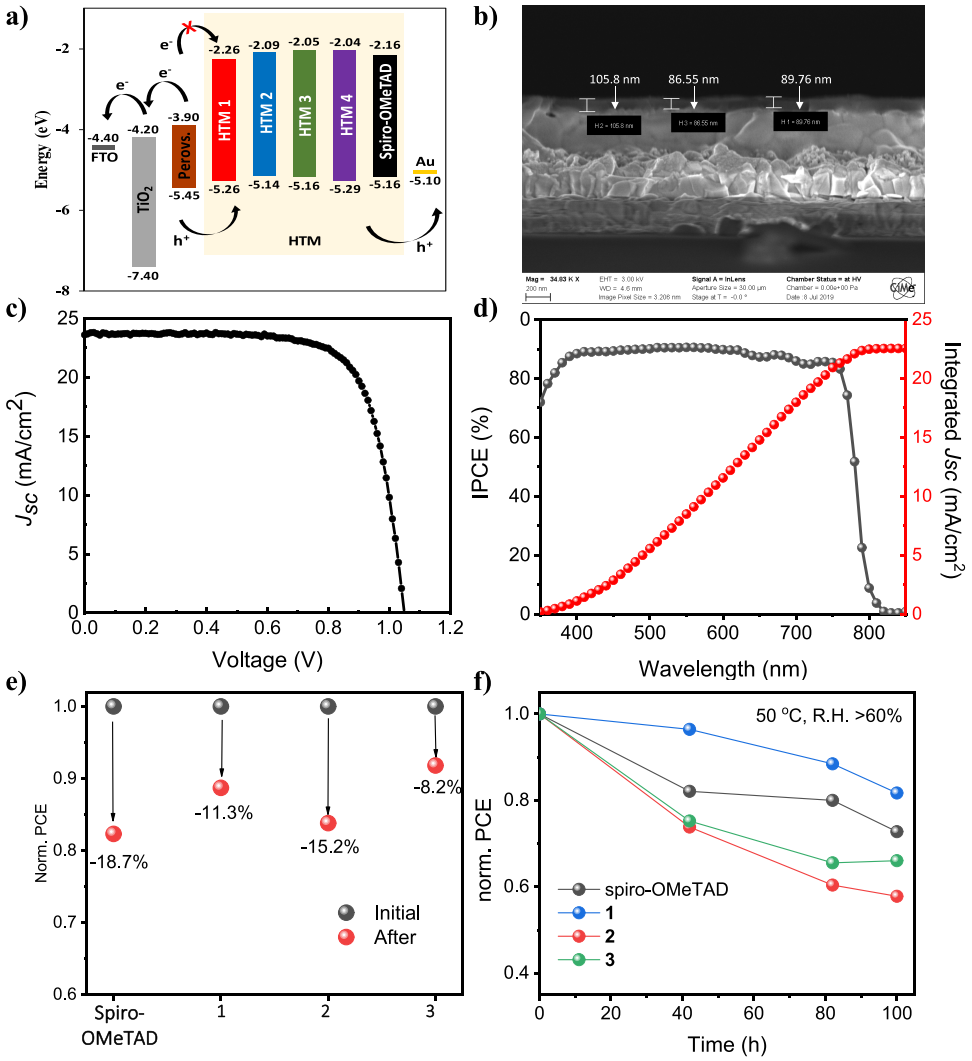

Figure 4. (a) Energy level diagram for the device layers. (b) Cross-section SEM image of devices for HTM **1** with Li-TFSI and *t*BP dopants. (c) Current density (J)−voltage (V) curve and (d) incident photon-to-current efficiency (IPCE) spectrum of the device with **1** employing Li-TFSI, *t*BP, and FK209 as additives. Stability performance of perovskite solar cell devices with different HTMs under (e) shelf conditions after 600 h and (f) thermal stress of 50 °C and relative humidity (R.H.) > 60% under darkness.

visible wavelengths. This is further confirmed as there is significant correlation between the center peak, full width at half maximum, and integrated spectrum, as shown in Table S11. Figure 2c shows the integrated ssPL spectra normalized to devices with pristine perovskite. Here, the different quenching effects of the HTMs on the photoluminescence are clearly seen. Compared to control devices, those with **2**, **3**, and **4** as HTMs luminesce more, indicating a less NRR. HTM **1**, on the other hand, shows an increased quenching, indicating an increased NRR as well. These results are further confirmed by the TRPL decays, in which **4** has the longest decay, corresponding to the one with the highest integrated ssPL.

https://doi.org/10.1021/acsaem.1c03775
ACS Appl. Energy Mater. 2022, 5, 3156−3165

Table 2. Best (Average ± Standard Deviation) Photovoltaic Parameters of Devices with 1, 2, 3, and 4 as Hole-Transporting Materials (HTMs)

HTM	J_{sc} (mA cm^{-2})[a]	V_{oc} (V)[a]	FF (%)[a]	PCE (%)[a]
spiro-OMeTAD	24.3 (24.3 ± 0.1)	1.10 (1.10 ± 0.01)	76.7 (75.0 ± 1.8)	20.7 (20.1 ± 0.5)
1	24.2 (24.1 ± 0.2)	1.02 (1.02 ± 0.01)	71.8 (69.4 ± 3.5)	17.7 (16.8 ± 1.0)
2	22.3 (22.1 ± 0.2)	1.02 (1.02 ± 0.00)	73.4 (72.0 ± 1.3)	16.7 (16.3 ± 0.3)
3	24.4 (24.2 ± 0.2)	1.06 (1.06 ± 0.01)	68.8 (65.2 ± 4.0)	17.8 (16.7 ± 1.1)
4	20.0 (19.0 ± 0.9)	1.00 (0.98 ± 0.01)	35.3 (31.2 ± 3.5)	7.1 (5.9 ± 0.9)

[a]Doped with Li-TFSI and *t*BP. The devices were measured under 100 mW·cm^{-2} Air-Mass 1.5G (AM1.5G) with simulated solar illumination 1.2 to 0.0 V. Eight devices were measured with each HTM.

HTMs **1**, **2**, **3**, and spiro-OMeTAD have similar curves, also corresponding to their integrated ssPL values (Figure 2d). So, compared to the isolated perovskite film, all of those with an HTM show significant quenching, pointing to effective charge extraction.

X-ray photoelectron spectroscopy (XPS) measurements were carried out to understand the interfacial interactions between the perovskite layer and HTLs. From the Pb perspective, all HTMs had coordination with Pb through O and S atoms. HTMs **1**, **2**, and **4** show a comparable but slightly stronger binding ability with Pb compared to spiro-OMeTAD (peak positions are slightly shifted to lower binding energies). HTM **3** had the strongest binding with Pb than the other HTMs (Figure 3a). Figure S21a shows that all HTMs have coordination between O and Pb in perovskite, evidenced by the peak shift to higher binding energies. Spiro-OMeTAD, **1**, and **3** are compared because they all have only O, which can coordinate with Pb in perovskite (Figure 3b). Both **1** and **3** show a higher binding energy of O than spiro-OMeTAD owing to the difference in the molecular structure, especially **1**. After the deposition of these three HTMs on top of perovskite, binding energies shifted to a higher eV, indicating a coordination between HTMs and the perovskite. The shift of the binding energy (ΔE) of spiro-OMeTAD is the highest among others when the binding energies between HTMs and perovskite/HTM are compared, meaning a stronger binding between the spiro-OMeTAD and the perovskite. Based on the measured ΔE, we can confirm the binding of S with perovskite and/or other molecules (Figure S21b,c).

Photovoltaic Devices. Based on photophysical and electrochemical properties, all the new HTMs under study have favorable HOMO levels for the extraction of holes in the perovskite layer, as well as the LUMO suitable for effective blocking of the flow of electrons from the active layer (Figure 4a). PSCs were fabricated in order to investigate the overall photovoltaic performance of the novel HTMs by the configuration structure of FTO/compact-TiO_2/mesoporous-TiO_2/perovskite/HTM/Au. The cross section of the PSC device was checked by scanning electron microscopy (SEM) with **1** in Figure 4b, where the thickness of the doped HTM layer was estimated to be about 90 nm. The statistic box charts of the main four photovoltaic parameters are shown in Figure S22, and the photovoltaic metrics are summarized in Table 2. The devices for the statistics were prepared under the same conditions.

When molecules with methoxyphenyl groups are compared with their analogues with methylthiophenyl groups, a general worsening in the photovoltaic parameters is observed. HTM **4** is the derivative that has given the lowest photovoltaic values, probably due to the low hole mobility that it exhibits compared to the other materials, in addition to the poor surface coverage and inhomogeneity indicated in the SEM image, which creates severe recombination and pinholes at the interface with perovskite. Derivative **4** also exhibits the lowest V_{oc}, despite having the most negative HOMO. In fact, all materials offer a low experimental V_{oc} compared to the theoretical value, confirming that there are high unproductive interfacial recombination phenomena. According to the SEM images, derivative **1** presents a coverage similar to that of the reference material. Compounds **2** and **3** also show good coverage without pinholes (Figure S23).

The short-circuit photocurrent density (J_{sc}) of derivatives **2** and **4** are conspicuously low compared to those of the other HTMs, which can be related to the low hole mobilities in the films. Nevertheless, these results indicate that the introduction of novel HTMs **1**, **2**, and **3**, presented good photovoltaic performances of over 16.3% PCE in average, with **1**, **2**, and **3** being the best, having average PCEs of 16.8, 16.3, and 16.7%, respectively, and maxima PCEs of 17.7, 16.7, and 17.8%, respectively. Devices with HTMs **1** and **3** had similar J_{sc}, indicating that they extract the holes similarly, which agrees with the photoluminescence data. Although those containing **3** had a higher V_{oc} (1.06 V *vs* 1.02 V), those with **1** exhibited a higher FF (71.8% *vs* 68.8%), so resulting in similar PCEs. HTMs **1** and **3** are the most promising materials, so we are conducting further research. From the results, we can advance here the improvement of the performance of the **1**-based devices by also adding the well-known dopant FK209 (tris[2-((1*H*-pyrazol-1-yl)-4-*tert*-butylpyridine)cobalt(III)-tris(bis(trifluoromethylsulfonyl)imide)]), which facilitates the charge extraction.[47] A better performance of 18.2% was obtained, with a J_{sc} of 24.2 mA cm^{-2}, an open-circuit voltage of 1.07 V, and a fill factor (FF) of 72%, (Figure 4c). In the case of **3**, the FF was improved, but J_{sc} was reduced from 24.4 to 22.5 mA cm^{-2}, leading to a slight decrease in PCE (Table S12). The corresponding integrated incident photo-to-current efficiency (IPCE) spectrum for **1** is shown in Figure 4d.

Stability Studies. As stated before, the stability of PSCs is one of the most challenging parameters for practical application that must be addressed. The shelf stability of the devices with different HTMs, comparing them with control devices with spiro-OMeTAD, was evaluated over 600 h with a relative humidity (R.H.) of 20% under dark conditions. The stability of the devices with HTMs **1**, **2**, and **3** was characterized due to their relatively good performance. Devices with spiro-OMeTAD showed the lowest stability among the four materials under study (Figure 4e). It can be seen in Figure 4e that the PCE of the spiro-OMeTAD-based device has the most inferior stability, losing up to 19% of PCE after a 600 h experiment, which agrees with a preceding report,[48] unlike the devices based on the novel HTMs that presented a better long-term stability. The most stable ones were **1** and **3**, which

https://doi.org/10.1021/acsaem.1c03775
ACS Appl. Energy Mater. 2022, 5, 3156−3165

maintained around 90% efficiency after 600 h storage. Thermal stability tests of the devices with different HTMs were monitored by measuring their current density vs voltage (J–V) curves at regular time intervals at 50 °C under R.H. > 60% conditions for over 100 h, and the corresponding photovoltaic performances without any encapsulation are recorded, as shown in Figure 4f. After 100 h thermal stress in a humid atmosphere, the devices incorporating **1** exhibit the best stability preserving 85% PCE, whereas the PCEs of spiro-OMeTAD, **3**, and **2** drop by nearly 70, 65, and 60% under the same circumstance, respectively. After 100 h thermal stress in a humid atmosphere, the devices incorporating **1** exhibit the best stability preserving 85% PCE, whereas the PCEs of spiro-OMeTAD, **3**, and **2** drop by nearly 70, 65, and 60% under the same circumstance, respectively.

Continuing with thermal stability, a slight reduction in J_{sc} and V_{oc} was observed for almost all HTMs (see Figure S24), except for the V_{oc} of **1**, which might originate from the degradation of the perovskite and TiO_2–perovskite interfaces that has a serious effect on charge transfer at the interface.[30] In addition, there is a notable decrease in FF in the case of devices with HTMs **2** and **3**, while this parameter remains relatively constant in the devices with the reference HTM and the HTM **1**. This fact can be explained by the general deterioration of the devices, thus resulting in recombination phenomena and an increase in series resistance.[49] In the case of HTM **2**, there is a striking phenomenon, in which the FF improves after an initial worsening, a trend that is also followed by the PCE. This phenomenon can be attributed to the effect of doping with the gold coming from the electrode due to heating and because the gold particles present in the cracks that can cause shunts are rearranged with the heat treatment.[50]

These results indicated that among these new 3D non-fused structures, **1** exhibited a better thermal stability than the other counterparts, which was mainly due to its inherent hydrophobic property, as revealed by contact angle measurements, where the images of the deionized water droplets on the surfaces of different HTMs are illustrated in Figure 5.

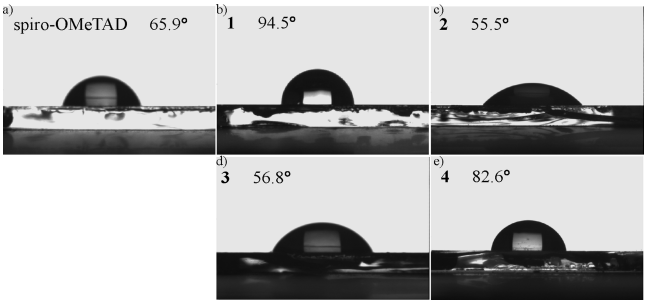

Figure 5. Contact angle measurements of (a) spiro-OMeTAD, (b) **1**, (c) **2**, (d) **3**, and (e) **4**.

Remarkably, a contact angle with water of 94.5° is obtained on the **1** surface, indicating a dramatic increase compared to spiro-OMeTAD and the other three novels HTMs, thereby resulting in an enhanced device stability under a humid atmosphere.

Above all, although it is necessary to conduct more rigorous stability tests, the stability results indicate that, for practical purposes, the trade-off between the efficiency and excellent long-term stability of new alternative HTMs is crucial for PSCs since most devices using spiro-OMeTAD are accompanied with serious degradation.

CONCLUSIONS

In summary, broad and organized of 3D non-fused asymmetric hole-transporting materials (HTMs) have been developed by tuning the position and type of heteroatom on the peripheral substituents to comprehensively understand their influences on the photovoltaic performance of the perovskite solar cells (PSCs). All four new materials have shown good solubility in common organic solvents, favoring their solution processing. Derivatives presenting the methoxyl substituent of the triphenylamine pending group in the *para* position (**1** and **2**) had a higher T_g and broader band gap than those that presented it in *meta* (**3** and **4**). Those derivatives with methylthio substituents attached on the diphenylamine rings at 2,7-positions of fluorene (**2** and **4**) showed deeper HOMOs and lower hole mobilities than those with methoxyls (**1** and **3**). Furthermore, systems with methylthio appear to form thin layers with worse morphology compared to those with methoxy instead. Indeed, **1** and **3** have led to the best photovoltaic results, with sunlight-to-electricity power conversion efficiencies (PCEs) of 17.7 and 17.8%, respectively, in the presence of dopants Li-TFSI and *t*BP. The new HTMs presented a lower photovoltaic performance than the reference material, mainly due to the lower hole mobility, consistent with theoretical calculations. A higher binding energy with Pb has been demonstrated by X-ray photoelectron spectroscopy for the new HTMs, especially for HTM **3**. Moreover, HTMs **1** and **3** have presented higher Pb–O binding energies than spiro-OMeTAD. Nevertheless, a stronger global binding between the spiro-OMeTAD and the perovskite was found, which agrees with the photovoltaic results. The results show an improvement up to 18.2% of the PCE for **1** upon doping with Li-TFSI, *t*BP, and FK209. Although devices based on spiro-OMeTAD was superior in photovoltaic performance, those with HTMs **1**, **2**, and **3** showed a better shelf and thermal stability than the devices with the reference HTM. The new materials described here are less expensive to synthesize and purify than the widely used spiro-OMeTAD, in addition to the better long-term stability of the resulting PSCs. Finally, it has been observed that those derivatives containing methylthio substituents in their structure (**2** and **4**) give rise to a poorer photovoltaic performance when applied as HTMs, probably because the morphology of the films is less suitable, which worsens when methoxyl groups are in the *meta* position. However, if HTMs including only methoxy groups in their structure (**1** and **3**) are compared, it has been seen that in the presence of dopants Li-TFSI and *t*-BP, the best result is obtained from the derivative with methoxyls in *meta*. Nevertheless, when adding the dopant FK209, the best is the molecule with substituents in *para*, which leads us to think that in this case, the big difference is the oxidation state of the HTM. The results that we have obtained give us clues to the next step in the design of high-efficiency HTMs.

ASSOCIATED CONTENT

Supporting Information

The Supporting Information is available free of charge at https://pubs.acs.org/doi/10.1021/acsaem.1c03775.

Computational details, scheme of synthesis routes,[1] H NMR,[13] C NMR, HRMS, cost estimation of HTMs,

https://doi.org/10.1021/acsaem.1c03775
ACS Appl. Energy Mater. 2022, 5, 3156–3165

device fabrication, detailed device parameters of TRPL spectra, DSC, TGA, UV−Visible absorption in the solid state, SCLC curves, additional XPS analyses, statistic box charts for the photovoltaic parameters, SEM of the surface; and instrumentals for the tests (PDF)

AUTHOR INFORMATION

Corresponding Authors

Esmaeil Sheibani − *Department of Chemistry, University of Isfahan, Isfahan 81746-73441, Iran;* orcid.org/0000-0002-3790-6573; Email: e.sheibani@sci.ui.ac.ir; Fax: +98-31-36689732

Anders Hagfeldt − *Laboratory of Photomolecular Science, Institute of Chemical Sciences and Engineering, School of Basic Sciences, Ecole Polytechnique Fédérale de Lausanne, Lausanne CH-1015, Switzerland;* orcid.org/0000-0001-6725-8856; Email: anders.hagfeldt@uu.se

Authors

Desire Molina − *Laboratory of Photomolecular Science, Institute of Chemical Sciences and Engineering, School of Basic Sciences, Ecole Polytechnique Fédérale de Lausanne, Lausanne CH-1015, Switzerland; División de Química Orgánica, Instituto de Bioingeniería, Universidad Miguel Hernández, Elche 03202, Spain*

Bowen Yang − *Laboratory of Photomolecular Science, Institute of Chemical Sciences and Engineering, School of Basic Sciences, Ecole Polytechnique Fédérale de Lausanne, Lausanne CH-1015, Switzerland;* orcid.org/0000-0002-9471-3452

Hajar Mohammadi − *Department of Chemistry, University of Isfahan, Isfahan 81746-73441, Iran*

Maryam Ghiasabadi − *Department of Chemistry, University of Isfahan, Isfahan 81746-73441, Iran*

Bo Xu − *MIIT Key Laboratory of Advanced Display Materials and Devices, Institute of Optoelectronics & Nanomaterials, College of Materials Science and Engineering, Nanjing University of Science and Technology, Nanjing 210094, China;* orcid.org/0000-0002-4703-7340

Jiajia Suo − *Laboratory of Photomolecular Science, Institute of Chemical Sciences and Engineering, School of Basic Sciences, Ecole Polytechnique Fédérale de Lausanne, Lausanne CH-1015, Switzerland*

Brian Carlsen − *Laboratory of Photomolecular Science, Institute of Chemical Sciences and Engineering, School of Basic Sciences, Ecole Polytechnique Fédérale de Lausanne, Lausanne CH-1015, Switzerland*

Nick Vlachopoulos − *Laboratory of Photomolecular Science, Institute of Chemical Sciences and Engineering, School of Basic Sciences, Ecole Polytechnique Fédérale de Lausanne, Lausanne CH-1015, Switzerland*

Shaik Mohammed Zakeeruddin − *Laboratory of Photonics and Interfaces, Institute of Chemical Sciences and Engineering, School of Basic Sciences, Ecole Polytechnique Fédérale de Lausanne, Lausanne CH-1015, Switzerland*

Michael Grätzel − *Laboratory of Photonics and Interfaces, Institute of Chemical Sciences and Engineering, School of Basic Sciences, Ecole Polytechnique Fédérale de Lausanne, Lausanne CH-1015, Switzerland;* orcid.org/0000-0002-0068-0195

Complete contact information is available at: https://pubs.acs.org/10.1021/acsaem.1c03775

Notes

The authors declare no competing financial interest.

ACKNOWLEDGMENTS

B.Y. acknowledges the financial support from the European Union's Horizon 2020 Framework Programme under grant agreement No 764047. D. M. thanks the European Social Fund for the grant APOSTD/2017/026. E.S. thanks the Iran National Science Foundation (INSF, grant no. 98016555) and University of Isfahan for financial support this project. All the authors thank Ángela Sastre-Santos for lending her facilities to measure the UV−Vis spectra on the films of the new HTMs.

REFERENCES

(1) Jiang, Q.; Zhao, Y.; Zhang, X.; Yang, X.; Chen, Y.; Chu, Z.; Ye, Q.; Li, X.; Yin, Z.; You, J. Surface Passivation of Perovskite Film for Efficient Solar Cells. *Nat. Photonics* **2019**, *13*, 460.

(2) Turren-Cruz, S.-H.; Hagfeldt, A.; Saliba, M. Methylammonium-Free, High-Performance, and Stable Perovskite Solar Cells on a Planar Architecture. *Science* **2018**, *362*, 449−453.

(3) Bi, D.; Yi, C.; Luo, J.; Décoppet, J.-D.; Zhang, F.; Zakeeruddin, S. M.; Li, X.; Hagfeldt, A.; Grätzel, M. Polymer-Templated Nucleation and Crystal Growth of Perovskite Films for Solar Cells with Efficiency Greater Than 21%. *Nat. Energy* **2016**, *1*, 16142.

(4) Bi, D.; Tress, W.; Dar, M. I.; Gao, P.; Luo, J.; Renevier, C.; Schenk, K.; Abate, A.; Giordano, F.; Baena, J.-P. C. Efficient Luminescent Solar Cells Based on Tailored Mixed-Cation Perovskites. *Sci. Adv.* **2016**, *2*, No. e1501170.

(5) Saliba, M.; Matsui, T.; Seo, J.-Y.; Domanski, K.; Correa-Baena, J.-P.; Nazeeruddin, M. K.; Zakeeruddin, S. M.; Tress, W.; Abate, A.; Hagfeldt, A.; Grätzel, M. Cesium-Containing Triple Cation Perovskite Solar Cells: Improved Stability, Reproducibility and High Efficiency. *Energy Environ. Sci.* **2016**, *9*, 1989−1997.

(6) Saliba, M.; Matsui, T.; Domanski, K.; Seo, J.-Y.; Ummadisingu, A.; Zakeeruddin, S. M.; Correa-Baena, J.-P.; Tress, W. R.; Abate, A.; Hagfeldt, A.; Grätzel, M. Incorporation of Rubidium Cations into Perovskite Solar Cells Improves Photovoltaic Performance. *Science* **2016**, *354*, 206−209.

(7) Correa-Baena, J.-P.; Tress, W.; Domanski, K.; Anaraki, E. H.; Turren-Cruz, S.-H.; Roose, B.; Boix, P. P.; Grätzel, M.; Saliba, M.; Abate, A.; Hagfeldt, A. Identifying and Suppressing Interfacial Recombination to Achieve High Open-Circuit Voltage in Perovskite Solar Cells. *Energy Environ. Sci.* **2017**, *10*, 1207−1212.

(8) Anaraki, E. H.; Kermanpur, A.; Steier, L.; Domanski, K.; Matsui, T.; Tress, W.; Saliba, M.; Abate, A.; Grätzel, M.; Hagfeldt, A.; Correa-Baena, J. P. Highly Efficient and Stable Planar Perovskite Solar Cells by Solution-Processed Tin Oxide. *Energy Environ. Sci.* **2016**, *9*, 3128−3134.

(9) Baena, J. P. C.; Steier, L.; Tress, W.; Saliba, M.; Neutzner, S.; Matsui, T.; Giordano, F.; Jacobsson, T. J.; Kandada, A. R. S.; Zakeeruddin, S. M. Highly Efficient Planar Perovskite Solar Cells through Band Alignment Engineering. *Energy Environ. Sci.* **2015**, *8*, 2928−2934.

(10) Park, S. M.; Mazza, S. M.; Liang, Z.; Abtahi, A.; Boehm, A. M.; Parkin, S. R.; Anthony, J. E.; Graham, K. R. Processing Dependent Influence of the Hole Transport Layer Ionization Energy on Methylammonium Lead Iodide Perovskite Photovoltaics. *ACS Appl. Mater. Interfaces* **2018**, *10*, 15548−15557.

(11) Jiang, Q.; Zhang, L.; Wang, H.; Yang, X.; Meng, J.; Liu, H.; Yin, Z.; Wu, J.; Zhang, X.; You, J. Enhanced Electron Extraction Using Sno 2 for High-Efficiency Planar-Structure Hc (Nh 2) 2 Pbi 3-Based Perovskite Solar Cells. *Nat. Energy* **2017**, *2*, 1−7.

(12) Ke, W.; Fang, G.; Liu, Q.; Xiong, L.; Qin, P.; Tao, H.; Wang, J.; Lei, H.; Li, B.; Wan, J.; Yang, G.; Yan, Y. Low-Temperature Solution-Processed Tin Oxide as an Alternative Electron Transporting Layer for Efficient Perovskite Solar Cells. *J. Am. Chem. Soc.* **2015**, *137*, 6730−6733.

(13) Lee, J.-W.; Lee, S. H.; Ko, H.-S.; Kwon, J.; Park, J. H.; Kang, S. M.; Ahn, N.; Choi, M.; Kim, J. K.; Park, N.-G. Opto-Electronic Properties of Tio 2 Nanohelices with Embedded Hc (Nh 2) 2 Pbi 3 Perovskite Solar Cells. *J. Mater. Chem. A* **2015**, *3*, 9179−9186.
(14) Xu, B.; Sheibani, E.; Liu, P.; Zhang, J.; Tian, H.; Vlachopoulos, N.; Boschloo, G.; Kloo, L.; Hagfeldt, A.; Sun, L. Carbazole-Based Hole-Transport Materials for Efficient Solid-State Dye-Sensitized Solar Cells and Perovskite Solar Cells. *Adv. Mater.* **2014**, *26*, 6629−6634.
(15) Chen, Y. C.; Huang, S. K.; Li, S. S.; Tsai, Y. Y.; Chen, C. P.; Chen, C. W.; Chang, Y. J. Facilely Synthesized Spiro [Fluorene-9, 9′-Phenanthren-10′-One] in Donor−Acceptor−Donor Hole-Transporting Materials for Perovskite Solar Cells. *ChemSusChem* **2018**, *11*, 3225−3233.
(16) Magomedov, A.; Paek, S.; Gratia, P.; Kasparavicius, E.; Daskeviciene, M.; Kamarauskas, E.; Gruodis, A.; Jankauskas, V.; Kantminiene, K.; Cho, K. T.; Rakstys, K.; Malinauskas, T.; Getautis, V.; Nazeeruddin, M. K. Diphenylamine-Substituted Carbazole-Based Hole Transporting Materials for Perovskite Solar Cells: Influence of Isomeric Derivatives. *Adv. Funct. Mater.* **2018**, *28*, 1704351.
(17) Li, Y.; Zhu, R.; Wang, J.; Li, Z. S.; Xu, N.; Zhang, J.; Wang, P. N-Annulated Perylene-Based Hole Transporters for Perovskite Solar Cells: The Significant Influence of Lateral Substituents. *ChemSusChem* **2018**, *11*, 672−680.
(18) Sheibani, E.; Amini, M.; Heydari, M.; Ahangar, H.; Keshavarzi, R.; Zhang, J.; Mirkhani, V. Hole Transport Material Based on Modified N-Annulated Perylene for Efficient and Stable Perovskite Solar Cells. *Sol. Energy* **2019**, *194*, 279−285.
(19) Li, H.; Fu, K.; Hagfeldt, A.; Grätzel, M.; Mhaisalkar, S. G.; Grimsdale, A. C. A Simple 3, 4-Ethylenedioxythiophene Based Hole-Transporting Material for Perovskite Solar Cells. *Angew. Chem., Int. Ed.* **2014**, *53*, 4085−4088.
(20) Zhu, X. D.; Ma, X. J.; Wang, Y. K.; Li, Y.; Gao, C. H.; Wang, Z. K.; Jiang, Z. Q.; Liao, L. S. Hole-Transporting Materials Incorporating Carbazole into Spiro-Core for Highly Efficient Perovskite Solar Cells. *Adv. Funct. Mater.* **2019**, *29*, 1807094.
(21) Jeon, N. J.; Na, H.; Jung, E. H.; Yang, T.-Y.; Lee, Y. G.; Kim, G.; Shin, H.-W.; Seok, S. I.; Lee, J.; Seo, J. A Fluorene-Terminated Hole-Transporting Material for Highly Efficient and Stable Perovskite Solar Cells. *Nat. Energy* **2018**, *3*, 682−689.
(22) Bi, D.; Xu, B.; Gao, P.; Sun, L.; Grätzel, M.; Hagfeldt, A. Facile Synthesized Organic Hole Transporting Material for Perovskite Solar Cell with Efficiency of 19.8%. *Nano Energy* **2016**, *23*, 138−144.
(23) Lin, Y.-S.; Abate, S. Y.; Lai, K.-W.; Chu, C.-W.; Lin, Y.-D.; Tao, Y.-T.; Sun, S.-S. New Helicene-Type Hole-Transporting Molecules for High-Performance and Durable Perovskite Solar Cells. *ACS Appl. Mater. Interfaces* **2018**, *10*, 41439−41449.
(24) Chen, C.; Ding, X.; Li, H.; Cheng, M.; Li, H.; Xu, L.; Qiao, F.; Li, H. Highly Efficient Phenoxazine Core Unit Based Hole Transport Materials for Hysteresis-Free Perovskite Solar Cells. *ACS Appl. Mater. Interfaces* **2018**, *10*, 36608−36614.
(25) Zhang, F.; Wang, S.; Zhu, H.; Liu, X.; Liu, H.; Li, X.; Xiao, Y.; Zakeeruddin, S. M.; Grätzel, M. Impact of Peripheral Groups on Phenothiazine-Based Hole-Transporting Materials for Perovskite Solar Cells. *ACS Energy Lett.* **2018**, *3*, 1145−1152.
(26) Petrus, M. L.; Schutt, K.; Sirtl, M. T.; Hutter, E. M.; Closs, A. C.; Ball, J. M.; Bijleveld, J. C.; Petrozza, A.; Bein, T.; Dingemans, T. J.; Savenije, T. J.; Snaith, H.; Docampo, P. New Generation Hole Transporting Materials for Perovskite Solar Cells: Amide-Based Small-Molecules with Nonconjugated Backbones. *Adv. Energy Mater.* **2018**, *8*, 1801605.
(27) Liu, L.; Wu, Y.; Li, M.; Zong, X.; Sun, Z.; Liang, M.; Xue, S. Thieno [3, 2-B] Indole-Based Hole Transporting Materials for Perovskite Solar Cells with Photovoltages Exceeding 1.11 V. *Chem. Commun.* **2018**, *54*, 14025−14028.
(28) Simokaitiene, J.; Cekaviciute, M.; Baucyte, K.; Volyniuk, D.; Durgaryan, R.; Molina, D.; Yang, B.; Suo, J.; Kim, Y.; Filho, D. A.; Hagfeldt, A.; Sini, G.; Grazulevicius, J. V. d. S. Interfacial Versus Bulk Properties of Hole-Transporting Materials for Perovskite Solar Cells: Isomeric Triphenylamine-Based Enamines Versus Spiro-Ometad. *ACS Appl. Mater. Interfaces* **2021**, *13*, 21320−21330.
(29) Malinauskas, T.; Tomkute-Luksiene, D.; Sens, R. d.; Daskeviciene, M.; Send, R.; Wonneberger, H.; Jankauskas, V.; Bruder, I.; Getautis, V. Enhancing Thermal Stability and Lifetime of Solid-State Dye-Sensitized Solar Cells Via Molecular Engineering of the Hole-Transporting Material Spiro-Ometad. *ACS Appl. Mater. Interfaces* **2015**, *7*, 11107−11116.
(30) Rojas, D. E. M.; Cho, K. T.; Zhang, Y.; Urbani, M.; Tabet, N.; de la Torre, G.; Nazeeruddin, M. K.; Torres, T. Tetrathienoanthracene and Tetrathienylbenzene Derivatives as Hole-Transporting Materials for Perovskite Solar Cell. *Adv. Energy Mater.* **2018**, *8*, 1800681.
(31) Li, Y.; Scheel, K. R.; Clevenger, R. G.; Shou, W.; Pan, H.; Kilway, K. V.; Peng, Z. Highly Efficient and Stable Perovskite Solar Cells Using a Dopant-Free Inexpensive Small Molecule as the Hole-Transporting Material. *Adv. Energy Mater.* **2018**, *8*, 1801248.
(32) Sheibani, E.; Yang, L.; Zhang, J. Recent Advances in Organic Hole Transporting Materials for Perovskite Solar Cells. *Solar RRL* **2020**, *4*, 2000461.
(33) Molina-Ontoria, A.; Zimmermann, I.; Garcia-Benito, I.; Gratia, P.; Roldán-Carmona, C.; Aghazada, S.; Graetzel, M.; Nazeeruddin, M. K.; Martín, N. Benzotrithiophene-Based Hole-Transporting Materials for 18.2% Perovskite Solar Cells. *Angew. Chem., Int. Ed.* **2016**, *55*, 6270−6274.
(34) Xu, P.; Liu, P.; Li, Y.; Xu, B.; Kloo, L.; Sun, L.; Hua, Y. D−a−D-Typed Hole Transport Materials for Efficient Perovskite Solar Cells: Tuning Photovoltaic Properties Via the Acceptor Group. *ACS Appl. Mater. Interfaces* **2018**, *10*, 19697−19703.
(35) Sheibani, E.; Heydari, M.; Ahangar, H.; Mohammadi, H.; Fard, H. T.; Taghavinia, N.; Samadpour, M.; Tajabadi, F. 3d Asymmetric Carbozole Hole Transporting Materials for Perovskite Solar Cells. *Sol. Energy* **2019**, *189*, 404−411.
(36) SasiKumar, M.; Maddala, G.; Ambapuram, M.; Subburu, M.; Vaidya, J. R.; Babu, S. N.; Chetti, P.; Mitty, R.; Pola, S. Cost-Effective Thiophene-Assisted Novel Dopant-Free Hole Transport Materials for Efficient Perovskite Solar Cell Performance. *Sustainable Energy Fuels* **2020**, *4*, 4754−4767.
(37) Leijtens, T.; Ding, I.-K.; Giovenzana, T.; Bloking, J. T.; McGehee, M. D.; Sellinger, A. Hole Transport Materials with Low Glass Transition Temperatures and High Solubility for Application in Solid-State Dye-Sensitized Solar Cells. *ACS Nano* **2012**, *6*, 1455−1462.
(38) Wang, H.; Sheikh, A. D.; Feng, Q.; Li, F.; Chen, Y.; Yu, W.; Alarousu, E.; Ma, C.; Haque, M. A.; Shi, D.; Wang, Z. S.; Mohammed, O. F.; Bakr, O. M.; Wu, T. Facile Synthesis and High Performance of a New Carbazole-Based Hole-Transporting Material for Hybrid Perovskite Solar Cells. *ACS Photonics* **2015**, *2*, 849−855.
(39) Wang, L.; Sheibani, E.; Guo, Y.; Zhang, W.; Li, Y.; Liu, P.; Xu, B.; Kloo, L.; Sun, L. Impact of Linking Topology on the Properties of Carbazole-Based Hole-Transport Materials and Their Application in Solid-State Mesoscopic Solar Cells. *Solar RRL* **2019**, *3*, 1900196.
(40) Belisle, R. A.; Jain, P.; Prasanna, R.; Leijtens, T.; McGehee, M. D. Minimal Effect of the Hole-Transport Material Ionization Potential on the Open-Circuit Voltage of Perovskite Solar Cells. *ACS Energy Lett.* **2016**, *1*, 556−560.
(41) Shi, J.; Xu, X.; Li, D.; Meng, Q. Interfaces in Perovskite Solar Cells. *Small* **2015**, *11*, 2472−2486.
(42) Dänekamp, B.; Droseros, N.; Tsokkou, D.; Brehm, V.; Boix, P. P.; Sessolo, M.; Banerji, N.; Bolink, H. J. Influence of Hole Transport Material Ionization Energy on the Performance of Perovskite Solar Cells. *J. Mater. Chem. C* **2019**, *7*, 523−527.
(43) Hammett, L. P. The Effect of Structure Upon the Reactions of Organic Compounds. Benzene Derivatives. *J. Am. Chem. Soc.* **1937**, *59*, 96−103.
(44) Jeon, N. J.; Lee, H. G.; Kim, Y. C.; Seo, J.; Noh, J. H.; Lee, J.; Seok, S. I. O-Methoxy Substituents in Spiro-Ometad for Efficient Inorganic−Organic Hybrid Perovskite Solar Cells. *J. Am. Chem. Soc.* **2014**, *136*, 7837−7840.

https://doi.org/10.1021/acsaem.1c03775
ACS Appl. Energy Mater. 2022, 5, 3156−3165

(45) Pavlishchuk, V. V.; Addison, A. W. Conversion Constants for Redox Potentials Measured Versus Different Reference Electrodes in Acetonitrile Solutions at 25 C. *Inorg. Chim. Acta* **2000**, *298*, 97−102.
(46) Wang, X.; Zhang, J.; Yu, S.; Yu, W.; Fu, P.; Liu, X.; Tu, D.; Guo, X.; Li, C. Lowering Molecular Symmetry to Improve the Morphological Properties of the Hole-Transport Layer for Stable Perovskite Solar Cells. *Angew. Chem., Int. Ed.* **2018**, *57*, 12529−12533.
(47) Noh, J. H.; Jeon, N. J.; Choi, Y. C.; Nazeeruddin, M. K.; Grätzel, M.; Seok, S. I. Nanostructured Tio_2/Ch_3 Nh_3 Pbi_3 Heterojunction Solar Cells Employing Spiro-Ometad/Co-Complex as Hole-Transporting Material. *J. Mater. Chem. A* **2013**, *1*, 11842−11847.
(48) Wang, Z.; McMeekin, D. P.; Sakai, N.; van Reenen, S.; Wojciechowski, K.; Patel, J. B.; Johnston, M. B.; Snaith, H. J. Efficient and Air-Stable Mixed-Cation Lead Mixed-Halide Perovskite Solar Cells with N-Doped Organic Electron Extraction Layers. *Adv. Mater.* **2017**, *29*, 1604186.
(49) Wu, N.; Wu, Y.; Walter, D.; Shen, H.; Duong, T.; Grant, D.; Barugkin, C.; Fu, X.; Peng, J.; White, T.; Catchpole, K.; Weber, K. Identifying the Cause of Voltage and Fill Factor Losses in Perovskite Solar Cells by Using Luminescence Measurements. *Energy Technol.* **2017**, *5*, 1827−1835.
(50) Molina, D.; Ruiz-Preciado, M. A.; Carlsen, B.; Eickemeyer, F. T.; Yang, B.; Flores-Díaz, N.; Álvaro-Martins, M. J.; Nonomura, K.; Hagfeldt, A.; Sastre-Santos, Á. Zinc Phthalocyanine Conjugated Dimers as Efficient Dopant-Free Hole Transporting Materials in Perovskite Solar Cells. *ChemPhotoChem* **2020**, *4*, 307−314.

NOTE ADDED AFTER ASAP PUBLICATION

This was paper published on February 18, 2022. Desire Molina's name has been corrected and the paper was re-posted on March 15, 2022.

https://doi.org/10.1021/acsaem.1c03775
ACS Appl. Energy Mater. 2022, 5, 3156−3165